Modeling exponential decay in maximum capacitance across specified flight patterns in small aircraft

Pete B. Rigas[1], and Chetan S. Kulkarni[2],

[1] *Cornell University, Ithaca, NY, 14850*
rigas.pete@gmail.com, pbr43@cornell.edu

[2] *KBR, Inc., NASA Ames Research Center, Moffett Field, CA, 94035, USA*
chetan.s.kulkarni@nasa.gov

ABSTRACT

To generate predictions for flight plans that experience anomalies, or unexpected mechanical failures in the engine due to a parasitic load in a specified stage of the flight that must return to its starting point of origin, we begin by describing the procedures by which a sequence of steps will be carried out to exponentially weigh the impact of different stages of a flight towards thermal strain on the capacitance $C_{\max}$ of the battery during each flight.

1. INTRODUCTION

In a previous 2014 work, [2], sought to improve methods of generating flight predictions for small aircraft, the methodology and approach that follows will generate flights predictions of a similar type, for flights with individual stages of specified duration, so as to improve the maintenance of batteries and other equipment that are involved in the aircraft throughout flight. Moreover, to avoid having to perform laboratory tests on batteries after a fixed number of flights within a cycle, the model heavily relies on a free parameter choice to model the expected decay of the capacitance of the battery. In Section **8** of the report, the β parameter choices listed in the table correspond to the numerical values of the parameter from which upper and lower bounds of exponential decay in the capacitance of the battery are generated, as quantities that can be interpreted and continuously varied for a wide range of flight patterns.

In contrast to the remaining flight time that is put forth in [2], the approach is also aimed towards quantifying the exponential decay in the maximum capacitance, due to a parasitic load that is inserted within a fixed stage of the flight, and imposed for the remaining duration of the flight. To categorically separate and study the rate of change of exponential decay of the maximum capacitance of different batteries, parasitic loads of exponential, or of polynomial, magnitude are computed for consistent choices of β parameters. From the *percentage* of the maximum capacitance that the battery is observed to hold after a given cycle, the exponential factor that is temporally weighed in the duration of all stages of the flight allows for broader prognostics reflection, pertaining not only to equipment maintenance but also to total duration of a flight, and the accompanying SOC. Other works, including [1], and [3]- [10], offer detailed discussions of either the experimental set up of tests which were used to test the accuracy of different numerical models, in addition to architectural schemes of offline battery maintenance, insofar as to further study capacitance degradation.

With example upper and lower bounds on the maximum capacitance decay for a wide variety of flights from different batteries in the publicly available HRF repository, the parameter choice and resulting numerical behavior provides a formalism through which experiments consisting of flights with either longer duration, more complicated pattern with a larger number of stages, or varying electromagnetic radiation in the ambient environment of the flight, can be accounted for through adjustment of the β parameter, within the power of the exponent.

2. MOTIVATION

To characterize different flight plans from which sets of predictions will be generated, the approach detailed below will:

- provide calculations of the time duration of each segment of a flight, depending on the magnitude of the current exerted by the engine over each time in-

terval, which will be determined by the current at the end of the flight that the engine asymptotically reaches in the final stages of each plan,

- introduce an exponentially decaying factor, whose magnitude is numerically determined by enforcing a summation, which is determined by a sequence of multiplicative, freely chosen parameters $\{\beta_i\}$, the minimum and maximum of which are not only chosen to be proportional to the duration of separate periods of the flight, but also to the magnitude of the change of the current in each corresponding stage of the flight,
- computing the Fourier coefficients and series of current versus time plots from a prescribed set of flight plan data, from which predictions for upcoming, **future** flight plans will be generated by correlating, from the change in the magnitude of the exponential factor that is used to model the decay in the maximum capacitance of the circuit across multiple flights, an admissible range of Fourier modes, given a polynomial approximation of the current versus time data by a root finding method which achieves an approximation of the current data, with the degree of the approximation dependent on the number of roots in the current versus time data after a horizontal translation towards the t axis.

Rigorously, the Fourier series representation of each flight plan is obtained by:

- approximating the temporal duration of each segment of an arbitrary flight plan through the individual steps which include:
  - fixing a coordinate axis to measure applicable sine **or** cosine modes of the Fourier series representation which will be enforced after a smooth, polynomial approximation to the stage of the flight has been determined,
  - computing a sufficient number of Fourier coefficients so that the corresponding Fourier series representation of the flight plan sufficiently represents all current measurements for each point in time of the real flight plan before introducing a Fourier series, obtainable through a suitable trigonometric basis$\{\sin(\frac{n\omega_0 t}{T}), \cos(\frac{n\omega_0 t}{T})\}_{n\in\mathbf{N}}$, where the normalizing period T used to compute the coefficient basis is the duration of the specified stage of the flight with n steps over which the smooth approximation is enforced, $T = \sum_{i=1}^{n} t_i$, which can be realized by ensuring that for all $t_i \in T$, given arbitrary flight segments T, the tolerance provided to the polynomial root finding method satisfies the pointwise difference condition $|R(t_i) - f(t_i)| < \epsilon$, where R is the recorded measurements of the current for each flight plan and f is the corresponding polynomial approximation of the real time data, for arbitrary $\epsilon > 0$,
  - numerically determining a threshold of the Fourier modes $\mathcal{N}$ for which the mean squared error, for a generalized Fourier series $\sum_n a_n^2 + b_n^2$, or alternatively, $\sum_n a_n^2$ or $\sum_n b_n^2$, for Fourier cosine and sine series, respectively, beyond which the aforementioned summations does not substantially decrease, and hence, do not pose significant benefits towards generating more informative and reliable predictions.

Next, given such a Fourier series representation of the flight plan after a suitable polynomial approximation, in addition to the exponentially decaying factor for computing the change in the maximum and minimum capacitance that will be defined, the approach will generate predictions for flights plans of the following types, all of which are dependent on the duration of the specific stage of the flight, as well as the time stamp throughout the stage of the flight at which the plan is to be terminated.

- Flight Plan Type A: Given a set of experimental trials, it will be demonstrated how to compute an accompanying rate of exponential decay in the maximum capacitance over successive flights that is proportional to the magnitude, and duration, of the thermal stress and accordingly, the mechanical work, that is applied to the engine for each flight. From this factor, predictions will be readily generated for flights that are terminated in the beginning stages of a flight by:
  - computing the exponential decay of the maximum capacitance $C_{\max}$ across subsequent flights,
  - computing the **decrease** in $\mathcal{N}$ that is requisite to satisfy the piecewise conditions for R and f, which formally can be realized by incorporating, on average per segment of each flight, a specified number of Fourier modes in the series representation of the flight plan, which can be used to accommodate predictions for different time stamps throughout a fixed stage of a flight by continuously varying the rightmost endpoint in time on which the polynomial root finding method generates smooth approximations from the experimental current versus time data.
- Flight Plan Type B: Given a set of experimental trials, predictions for more complicated flight patterns can be generated by making use of the predictions

generated for flights of the previously defined type, in the sense that a flight pattern of Type B can be analyzed, from predictions of fights of Type A by implementing:

  - a prescribed number Fourier modes $\mathcal{N}$ in the series approximation in the beginning phase of the flight during which a current is beginning to flow in the circuit of the engine, from which predictions of a termination of the flight plan in the next stage of the flight, hence the name Type B, can be generated implementing the change in maximum capacitance from the previous flight plan, in addition to the minimum and maximum rates of exponential decay in $C_{\max}$, granted that the smooth polynomial approximation not violate the piecewise condition that $|R(t_i) - f(t_i)| < \epsilon$ for all times t_i preceding the unforseen abortion of the flight in its earlier stage.

- Flight Plans Types C,D,E: Repeating the same observations and formulations for flight plants of Type A and Type B mutatis mutandis gives immediate generalizations of other flight plans for which the unforseen abortion of the flight can occur. In particular, flight plans of Type C, Type D, and Type E, respectively, describe excursions on which the same maximum capacitance value (which is the $C_{\max}$ value computed from previous flights in a given sequence, determined from an initial capacitance value in the first flight of the sequence which we set to be at the 100% threshold), the final time stamp t_f are which the flight is terminated, as well as the accompanying number of Fourier modes in the series representation, inclusive of all stages of the flight that were completed under the specified plan.
- Flight Plan Type X; Pursuant of further generalizations, the preceding observations and formalism can be applied mutatis mutandis to new flights patterns, of emerging interest, for an arbitrary but countable number of intervals over which a flight can be terminated. Implementationwise, with numerical results surrounding the relationship between the mean square error and modes $\mathcal{N}$ that are to be presented, we will give a precise sense of the range of Fourier modes that will simultaneously provide reliable predictions for flight patterns of a given type, in addition to not being computationally expensive.

3. OVERVIEW OF THE APPROACH

3.1. Free parameters

To test the Fourier series and exponentially decaying capacitance factor to calculate the change in $C_{\max}$ values across successive flights, given a set of training data through a given sequence of flights beforehand, the approach will be implemented by executing the following steps:

- Running an auxiliary algorithm in Matlab which will return the **approximate time intervals**, and respective durations, of each stage of a given flight, which will be dealt with in two of the following cases:
  - **Case 1: (Flight plans in which the ending current reading for the final stage of the flight vertically asymptotes to values higher than those in preceding stages of the flight)** For flight plans of Case 1, one can easily generate time intervals for the intermediate stages of the flight plan by extending a horizontal line and linearly searching below such a threshold to obtain isolated segments of the flight during which polynomial approximations via the root finding method can be determined. From the current value that is exerted near the end of the flight from which the horizontal line is extended, a threshold δ will be chosen so that all current values below those of $\mathcal{H} - \delta$ will be returned.

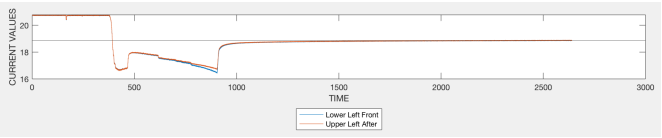

(ABOVE) *Figure 1*: Example of Set 6, HRF 77, plot of horizontal line for flight plan of Case 1, (BELOW) *Figure 2*: Plot of individual stages of the flight which are determined by linear inspection of the data through a specified threshold δ of the current asymptotic value given by the horizontal line at the end of the flight

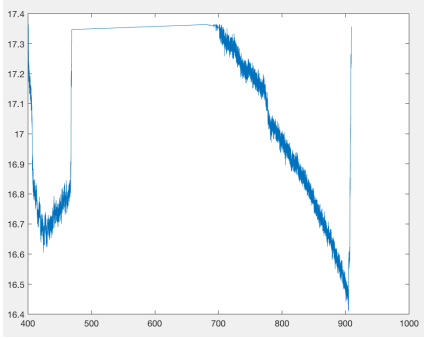

- **Case 2: (Flight plans in which the ending current reading for the final stage of the flight vertically asymptotes to values lower than those in the preceding stages of the flight)** For flight plans of Case 2, one can still generate analogous results corresponding to the time intervals for disjoint segments of a given flight plan, instead by enforcing that we linearly search **above** the current value that the data asymptotically approaches at the final time stamp of the given flight, while simultaneously conditioning that the search also enforce the criterion that the isolated segments of the flight, of Case 2, not exceed the initial current starting value at the beginning of the flight. After executing such a search, the auxiliary algorithm will similarly return a set of times for each stage of the flight, from which exponentially decaying factors temporally weighed in each stage of the flight can be calculated.

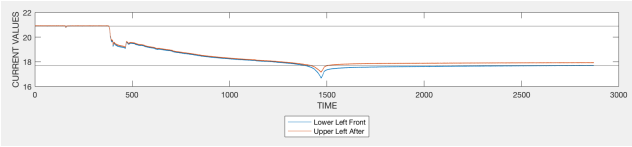

(ABOVE) *Figure 3*: Example of Set 6, HRF 80, plot of two horizontal lines for flight plan of Case 2, (BELOW) *Figure 4*: Plot of individual stages of the flight which are determined by linear inspection of the data through a specified threshold δ' of the current asymptotic value given by the horizontal line at the end of the flight

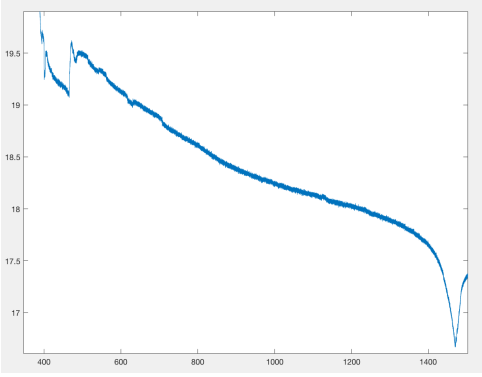

- Algorithmically determining, from the return values of the auxiliary algorithm, the estimated time intervals of each stage of the sequence of flights will be fed into the exponentially decaying factor in time that measures the change in $C_{\max}$ value across subsequent flights, from which the number of modes $\mathcal{N}$ for each period of the flight will be determined, with an accompanying MSE. From the chosen flight examples above, we observe that:

- From Set 6, HRF 77, disregarding the middle portion of the flight during which the magnitude of the current exerted on the current is approximately constant, one may compute the exponential decay in $C_{\max}$ by choosing suitable β_i, which in the case of this specific flight plan correspond to the real parameters that are linearly weighed in the temporal duration of the segments of the flight that occur between, respectively, before and after, the segment in which the current exerted on the engine in constant, so as to quantitatively determine the steepness of the decrease in $C_{\max}$ between subsequent flights. Notably, because the individual temporal factors in the exponentially decaying factor are inspired from straightforward solutions to one dimensional separable differential equations, if one were to temporally deform the first segment of the flight from Set 6, HRF 77 above, the expected exponential decay in $C_{\max}$, in comparison to that presented below, would **further** reduce the change in capacitance on the second flight, as $C^{1\to 2}_{\max_1} \geq C^{1\to 2}_{\max_2} \Leftrightarrow |T^1_{6,77}| = |\{t_i \in T^1_{6,77}\}| \leq |T^2_{6,77}| = |\{t_j \in T^2_{6,77}\}|$, where $(C_{\max_2}, T^2)$ denote the capacitance and stage duration pair of a time deformation for the stage $T^1_{6,77}$, by linearly extending the duration of this stage of the flight forwards in time while maintaining current measurements within a tolerance σ of all recorded values within a sufficiently small neighborhood of time stamps within the respective stage.

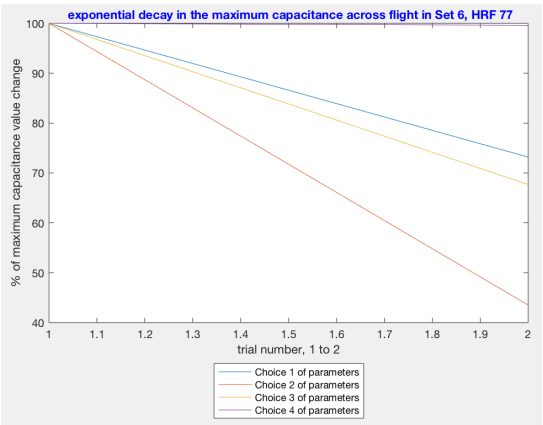

(ABOVE) *Figure 5*: From the two demarcated stages of the flight given the return values of the auxiliary algorithm, the exponential decay in $C_{\max}$ is exhibited across each stage of the flight. Because the beginning and ending stages of the flight have been removed by the auxiliary algorithm to provide approximate time intervals from which thermal stress on the engine is exhibited, which in turn results in the expected strain on the capacitance. To illustrate the dependence of the $C_{\max}$ value that we report based on the choice of each β_i.

case number	choice of parameters
1	$\beta_1 = \frac{1}{500}, \beta_2 = \frac{1}{5000}$
2	$\beta_1 = \frac{1}{100}, \beta_2 = \frac{1}{5000}$,
3	$\beta_1 = \frac{1}{2500} = \beta_2$
4	$\beta_1 = \frac{1}{25000}, \beta_2 = \frac{1}{25000}$

$C_{\max}$ value on flight 2
$C_{\max} \approx 0.73184 C_1$
$C_{\max} \approx 0.43509 C_1$,
$C_{\max} \approx 0.67686 C_1$
$C_{\max} \approx 0.99610 C_1$

(ABOVE) *Table 1*: Table providing choice of parameters for each of the 4 cases in the plot.

- On the other hand, from Set 6, HRF 80, the return values of time allow for calculations of the exponential decay in $C_{\max}$ for flights of Case 2. From noticeable differences in the trajectory of the flight from Set 6, the exponential decay in $C_{\max}$ is more sharp across the sequence of flights from that of HRF 80, primarily because the algorithm returns the collection of times corresponding to the current measurements that do not constantly vary with time. Therefore, the exponentially decaying constant not only penalizes the value of $C_{\max}$ in subsequent flights for sections of preceding flight plans for which there are nonzero changes in the current over prolonged periods of time, but also establishes how steep the rate of exponential decay is across a sequence of flights, from which predictions will be readily generated by incorporating bounds for $C_{\max}$ in the flight from which predictions will be generated.

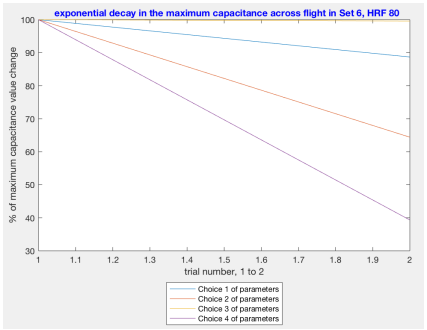

(ABOVE) *Figure 6*: From the two demarcated stages of the flight given the return values of the auxiliary algorithm, the exponential decay in $C_{\max}$ is exhibited across different stages of this flight. Significantly, in comparison to the exponential decay that has been calculated from the previous flight of Case 1, we conclude that the $C_{\max}$, albeit decaying across both flights, decays more robust decay across the second flight because the temporal duration of the second stage of the flight, weighed by the multiplicative parameter β_2, is larger in magnitude in comparison to the β_2 parameter introduced for the second stage of the flight in Set 6, HRF 77. As with the previous plot of the decay in $C_{\max}$, we introduce additional rates of exponential decay of $C_{\max}$, each of which are dependent on the specific choice of the β_i enforced throughout each stage of the flight.

case number	choice of parameters
1	$\beta_1 = \frac{1}{1000}, \beta_2 = \frac{1}{5000}$
2	$\beta_1 = \frac{1}{200}, \beta_2 = \frac{1}{5000}$,
3	$\beta_1 = \frac{1}{300000}, \beta_2 = \frac{1}{50000}$
4	$\beta_1 = \frac{1}{300} = \beta_2$

$C_{\max}$ value after flight 2
$C_{\max} \approx 0.88692 C_1$
$C_{\max} \approx 0.644036 C_1$,
$C_{\max} \approx 0.995742 C_1$
$C_{\max} \approx 0.99610 C_1$

(ABOVE) *Table 2*: Table providing choice of parameters for each of the 4 cases in the plot.

- Finally, to establish sets of predictions for flight of varying types, namely flights that have previously defined histories each of which have been defined, a Fourier series expansion will be introduced by computing the Fourier coefficients. With the essential smooth polynomial approximation of the flight data,

computational simulations of varying modes $\mathcal{N}$ in the expansion will be compared, as to determine an informative, yet computationally accessible, series expansion towards generating flight predictions.

3.2. Exponentially decaying capacitance

With the difference choices of β parameters that will be further expounded upon in more sensitive calculations of the exponential decay in $C_{\max}$ that are inclusive of the beginning and ending periods of the flight, we will make the choice of free β parameters so that the decay of the maximum capacitance between neighboring flights reflects a rate of decay in the capacitance that is appropriate, in the sense that the rate of exponential decay does not fall into any one of the cases above in which the maximum capacitance in one flight from a previous one is almost left unchanged, at or around 99% of the previous $C_{\max}$, or at around 50% of the $C_{\max}$ for a typical flight.

4. WORKFLOW

Before proceeding with more details, the cartoon below provides a high level summary of each step in the approach.

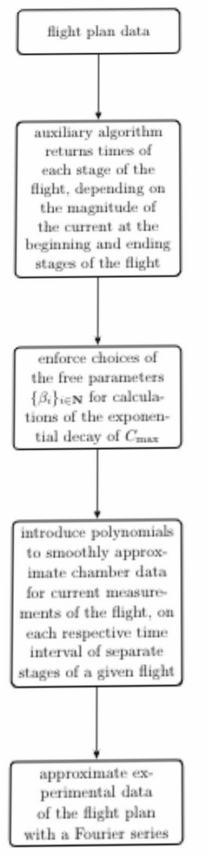

4.1. Implementations for Polynomial fitting

From standard polynomial fitting techniques, after making use of the auxiliary algorithm to obtain the time intervals of each stage over the flight in question between the beginning and final stages, a piecewise, smooth and

differentiable function can be fitted to the flight data through:

- A polynomial approximation to the data introduced through a Lagrange interpolating basis $\mathcal{L}$, of the form

$$\mathcal{L}_{n,j}(x) = \prod_{k \neq j} \frac{x - x_k}{x_j - x_k} \, ,$$

  for admissible points x, x_k, x_j lying within the time interval over the specified stage of the flight over which the polynomial approximation to the flight data is to be enforced, in which the basis functions over each stage of the flight above present a suitable approximation to a polynomial of degree n, given $n+1$ points. By construction, because the interpolating polynomial cannot exceed the $n-1$ points used to construct the basis, and in turn the linear combination has $\sum_{j=0}^{\mathcal{N}} \mathcal{I}_{t_j} \mathcal{L}_{n,j}(x)$, we will supply the interpolating polynomial with the sequence of experimentally measured currents $\mathcal{I}_{t_1^{(1)}}, \cdots, \mathcal{I}_{t_n^{(1)}}, \cdots, \mathcal{I}_{t_1^{(n)}}, \cdots, \mathcal{I}_{t_n^{(n)}}$, for arbitrary flight plans with n stages, to construct individual interpolating polynomials for each of the n stages. From such a collection of interpolating polynomials between subsequent stages of each flight the corresponding linear combinations $p^{(i)}(x), \cdots, p^{(j)}(x)$, each of which respectively correspond to the basis functions corresponding to the polynomials during stages $i, j < n$ of an arbitrary flight plan, will be chosen so that on the boundary points of neighboring stages of each flight, the interpolating polynomials on neighboring stages of the flight will agree on the final time $t_{\text{final}}^{(i)}$ corresponding to the stage $\mathcal{T}^{(i)}$, and initial time $t_{\text{initial}}^{(j)}$ for the stage $\mathcal{T}^{(j)}$. Altogether, after following the steps to construct the time intervals of each stage by the auxiliary algorithm, in addition to the steps detailed in the preceding remarks to construct a set of Lagrange interpolating basis $\{\mathcal{L}_{n,j}^{(i)}(x)\}_{n^i = |\mathcal{T}^{(i)}, 1 \leq j^{(i)} \leq n^{(i)}}$ corresponding to the polynomial approximation for stage $\mathcal{T}^{(i)}$, one may smoothly transform collected, real time flight data towards the objective of establishing predictions based on **either** anomalies in the flight plans or aircraft maintenance.
- To address shortcomings of the Lagrange interpolating basis in Matlab, in which polynomials obtained through the polyfit method fail to pass through the points that are supplied as initial data points because coefficients of the polynomial returned by the method become arbitrarily large, we will implement:
  - a polynomial root finding algorithm through a suitable linear translation of the data so as to represent the current versus time readings as a continuous polynomial that crosses the t axis a fixed number of times,
  - in addition to passing the smooth polynomials to compute the Fourier coefficients, and hence the Fourier series expansion, in which the Fourier coefficients are of the form,

$$a_n = \frac{1}{\sum_i t_i} \int_{t=0}^{T} f^{(i)}(t) \cos\left(\frac{2\pi n t}{T}\right) \mathrm{d}t \, ,$$

    and

$$b_n = \frac{1}{\sum_i t_i} \int_{t=0}^{T} f^{(i)}(t) \sin\left(\frac{2\pi n t}{T}\right) \mathrm{d}t \, .$$

4.2. Polynomial fitting: Root finding algorithm

Preliminarily, we will choose trials of subsequent flights from publicly available HRF data sets, from which the time intervals of each flight will be approximated. After having run the auxiliary algorithm to obtain intervals of time for each stage of the flight as previously demonstrated through the examples of HRF 77 and HRF 80 from Set 6, we implement a standard root finding procedure to obtain smooth polynomial approximations of the current readings on each interval of time, from which we will compute the Fourier series coefficients, and hence, the Fourier series expansion to generate flight predictions.

With a number of modes $\mathcal{N}$ defined over individual stages of a given flight, we will generate flight predictions for future flights by varying the location of the time stamp at which the flight is to be terminated. Concretely, if we continue with the running example that we have obtained with return times from the auxiliary algorithm, we can obtain smooth polynomial approximations by implementing the following steps:

- Examine the current versus time data to determine a suitable constant $\mathcal{C}$, and accompanying linear transformation φ so that all of the current data can be shifted down towards the t axis, insofar as to produce a collection of current versus time data that can be approximated with a root finding algorithm,
- Specify the degree of the smooth polynomial that will be used to approximate the current versus time data after the transformation φ is applied to shift the

data downards to the t axis, from which the degree of the approximation depends,

- Obtain the polynomial approximation for the flight interval over the specified duration of the stage of the flight, after incorporating a specified tolerance for the desired error between the polynomial approximation and the flight data. To avoid technicalities with the resulting polynomial approximation having roots over **C**, which would hence make it not make the analytic expression viable for future flight predictions, avoid choosing tolerances for the root finding algorithm which return a polynomial that does not have real roots.

To demonstrate the tradeoff between the maximum degree that one can expect from such a polynomial approximation and the tolerance that one enforces in the root finding method, the plots below demonstrate the trade off between various approximation methods.

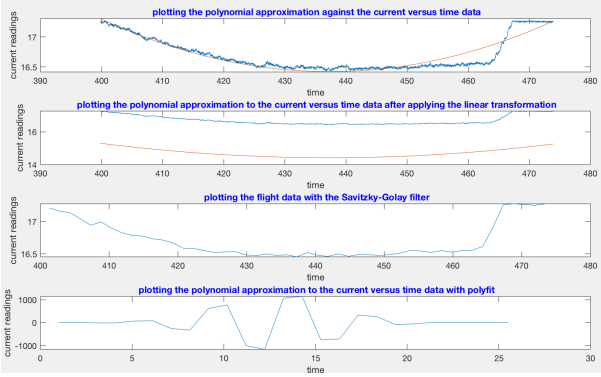

(ABOVE) *Figure 7*: The plot above demonstrates various approaches that one could use to generate polynomial approximations of flight data. In the first plot, the most reliable method is depicted, in which the polynomial root finding method determines the number of zeros of the current versus time data after the linear transformation is applied to translate the current readings so that a sufficient number of zeros occur on the t axis for the polynomial root finding algorithm to successfully introduce a second degree polynomial approximation with two roots r_1 and r_2, in addition to a stretching constant k. In the second plot, the polynomial approximation to the current versus time flight data is depicted before the approximation is shifted above the t axis to its normal position before the transformation is applied. In the third plot, the SGO filter is applied to the current versus time readings, which provides a flawless, smooth approximation for all sections of this given stage of the flight plan, but fails to be ideal because it does not provide an exact analytic expression for the polynomial approximation that is necessary for computations involving the Fourier coefficients, and the Fourier series, in future steps. In the fourth plot, the polyfit function is used to obtain an approximation of the current versus time readings. Across the 80 time stamp duration of this stage of the flight, this method is the worse of the previous 3, because although the function is able to return coefficients of a polynomial of degree 80 that can approximate the flight data, the curvature of the polynomial is very non smooth, in addition to the analytic expression for the approximation failing to capture the specified values of the current readings at time stamps throughout the stage of the flight. To improve upon flight predictions that are generated based on akin polynomial approximations for individual stages of different flights as the one produced above from the polynomial root finding method, we will implement a step function to account for the change in current between neighboring stages of a given flight.

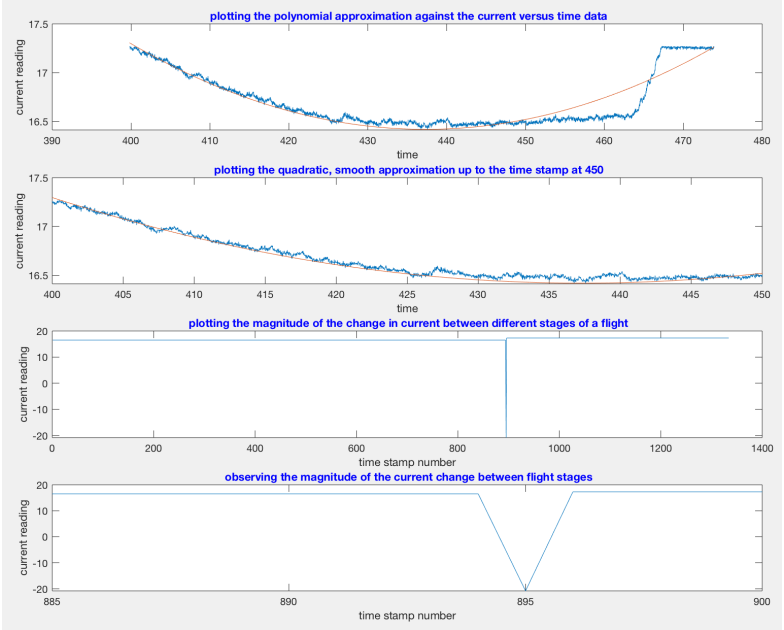

(ABOVE) *Figure 8*: To incorporate further improvements on the polynomial approximation of the flight data, the first plot above demonstrates the complete polynomial approximation to the flight data that was presented on the previous page. With such a smooth approximation of the flight data, it is possible to generate predictions up to the time stamp at 450 because the quadratic approximation nearly perfectly captures the sinusoidal like oscillation of the current measurement readings. However, due to inefficiencies in the polyfit method, in addition to the polynomial root finding meth-

ods, predictions for this example flight will only be generated up to time stamp 450 at which the approximation is enforced, not only because the approximation beyond this time stamp is not reflective of the non smooth, sudden jump in current that the engine undergoes between different stages of the flight. To accommodate this difficulty, the second plot above demonstrates the time stamp up to which the smooth polynomial approximation to the flight plan will be enforced, beyond which no predictions for this particular stage of the flight will be generated. On the other hand, we can also study the behavior and temporal duration of the current change between different stages of a flight by enforcing visually approximate values to the current behavior as the flux of current in the engine transitions to accommodate for changes in the flight plan. In the third plot above, approximate values for the experimentally gathered current readings are represented through the constant horizontal line, of value 16.5, while approximate values for the experimentally gathered current values after the current changes in magnitude for the termination of the first stage of the flight beyond the takeoff are approximated through the constant horizontal line of value 17.3. Altogether, the third plot demonstrate that there is a dramatic change in the value of the current readings between neighboring stages. In the {colororangefourth plot, the zoom in of the fourth plot above demonstrates how making use of the point slope formula to fit a line with positive slope for the current change, with one point centered at approximately time stamp 465 and another point centered at the time stamp approximately given by 466. After applying the point slope formula towards the function handle and evaluating it over all admissible time stamps during which the current change occurs, with the slope roughly given by $m \approx \frac{17.24-16.54}{467.2-463.5} \approx 0.189$, with the accompanying point slope formula, of the form $y \approx 0.189x+16.54$, the aforementioned expressions gives the linear change in behavior of the magnitude of the current that is accounted for.

4.3. Fourier series approach

With a polynomial approximation obtained via the root finding method, given an arbitrary number of time stamps before the flight plan is to be terminated, a modification to the usual Fourier sine and cosine coefficients will be introduced, in which each of the Fourier coefficients take the form,

$$a_n = \frac{1}{\sum_i t_i} \int_{\mathcal{T}_i} f(t)\cos\left(\frac{n\omega_0 t}{\mathcal{T}_i}\right)\mathrm{d}t \,,$$

and

$$b_n = \frac{1}{\sum_i t_i} \int_{\mathcal{T}_i} f(t)\sin\left(\frac{n\omega_0 t}{\mathcal{T}_i}\right)\mathrm{d}t \,,$$

where $\mathcal{T}$ denotes the stage of the flight over which the polynomial approximation has been obtained, and the normalizing constant for the period in the Fourier coefficients is the summation over all time stamps of the particular stage of the flight. As expected, f is smooth and from these expressions, one can obtain a series expansion of the form,

$$F(x) = \frac{a_0}{2} + \sum_{n,t\in\mathcal{T}_i} a_n\cos\left(\frac{n\omega_0 t}{\mathcal{T}_i}\right) + b_n\sin\left(\frac{n\omega_0 t}{\mathcal{T}_i}\right) \,,$$

where each period $\mathcal{T}_i$ is not only dependent on the duration of the time interval of the stage of the flight, but also on the current of the magnitude $\mathcal{I}$ exerted on the engine given a flight trajectory. With such a Fourier series that one can obtained from the aforementioned trigonometric basis, introduced over each respective $\mathcal{T}_i$, one can generate flight predictions for flight plans of Type A, for arbitrary time stamps t_j before the initial stage of the flight, by first introducing a polynomial approximation of the flight data up to t_j, and by then truncating the Fourier series expansion for $F(x)$, according to the maximum Fourier mode of the approximation which is determined to no longer substantially impact the MSE

$$\sum_n a_n^2 + b_n^2 \,,$$

of the approximation, where the truncation of the Fourier series takes the form,

$$F_{\mathcal{T}_i,t_i} = \frac{a_0}{2} + \sum_{n=1}^{\mathcal{M}_{t_i}} a_n\cos\left(\frac{n\omega_0 t}{\mathcal{T}_i}\right) + b_n\sin\left(\frac{n\omega_0 t}{\mathcal{T}_i}\right) \,,$$

for a sufficient number of modes $\mathcal{M}_{t_j} < \mathcal{N}$. With a series approximation $F_{\mathcal{T}_i,t_i}$ above denoting the series truncation corresponding to the maximum time stamp $t_i < t_j$ for which the 30% SOC threshold can be maintained when the flight is terminated at the later time t_j, for all $t \in \mathcal{T}_i$.

To ensure that such a truncation adequately captures the degradation in $C_{\max}$ across successive trials, or potentially across trials with a particular battery of some type, an exponentially decaying, temporally dependent factor, iterative factor is defined, of the form,

$$C_{\max_{i+1}} = e^{-\beta_1|t_i - t_j| - \beta_2|t'_i - t'_j|} C_{\max} \, ,$$

for time stamps $t_i, t_j \in \mathcal{T}_i$, and $t'_i, t'_j \in \mathcal{T}_j$. The free parameters β_1, β_2, as demonstrated in plots for different decay rates of $C_{\max}$, multiplicatively accompany the time intervals $[t_i, t_f]$ and $[t'_i, t'_f]$, respectively over $\mathcal{T}_i$ and $\mathcal{T}_j$, during each of which a current of varying magnitude $\mathcal{I}$ is exerted. More **generally**, the power of the exponent is of the form $\sum_t \beta_i |\mathcal{T}_i|$, which takes into account for all stages, including the beginning and end of the flight, to be discussed in the **next** section for flights in **Set 3**.

From previous discussions in earlier sections, the auxiliary algorithm now comes into play to provide approximate time intervals, given a flight plan, where the series representation will be introduced, each of which are respectively defined on time intervals over which smooth function approximations are introduced. In complete generality, for an arbtirary number of stages in the flight in which the change in magnitude of $\mathcal{I}$ is large enough to warrant introducing **another** smooth approximation of a new stage of the flight, additional smooth functions $\{f_i\}_{i\in\mathbf{N}}$, each of are passed to Fourier coefficients a_{n_i}, b_{n_i}, constitute a basis for a Fourier series representation, with $\mathcal{N}_i$ modes. For distinct time periods of each stage of the flight, the rates of exponential decay in $C_{\max}$, in addition to the series representation, together provide flight predictions by:

- computing the rate of exponential decay in the $C_{\max}$ across multiple flights with specified duration from the periods $\mathcal{T}_1^1, \cdots, \mathcal{T}_n^1, \cdots, \mathcal{T}_N^1, \cdots, \mathcal{T}_N^n$,
- incorporating the exponential decay mentioned in the previous step to determine the maximum durations of time for which the flight can maintain the 30% threshold, with the formula

$$\text{SOC} = 1 - \frac{q_{\max} - q_b}{C_{\max}} \, ,$$

  provided for computing the threshold in Hogge et al, 2015,
- and finally, determining the range of admissible Fourier modes in the series representation and computing the MSE for the number of modes.

4.4. Computation Case Studies

*** examples of computations for the Fourier series coefficients, in addition to the corresponding MSE, for the quadratic smooth polynomial approximation to flight data given in previous discussions. Discuss this in the section. If already done then we can ignore it ***

Before carrying out such computations for different sets of HRF data, we will exhibit typical values for the MSE, depending on computations of the Fourier coefficients, for the quadratic approximation to the flight data that was obtained through the polynomial root finding method. With a substantial array of Fourier coefficients, ranging from 200, 2,000 to 10,000, all of which together constituted a run time of approximately 3 days, constituting numerical simulations from which properties of the convergence of Fourier series will be exhibited, particularly through the convergence of the MSE to a fixed, determinable quantity, that can be obtained without having to resort to the computation of more than a few thousand Fourier series coefficients.

table of Fourier coefficients for smooth polynomial approximation up to the final time stamp of the stage, $t = 473.3$

Table 3: **Fourier cosine coefficients**

number of Fourier modes	maximum Fourier mode	minimum Fourier mode
200	≈ 0.40793	$\approx 2.7658 \times 10^{-6}$
2,000	≈ 0.40793	$\approx 2.7049 \times 10^{-8}$
10,000	≈ 0.40793	$\approx 1.0955 \times 10^{-3}$

Table 4: **Fourier sine coefficients**

number of Fourier modes	maximum Fourier mode	minimum Fourier mode
200	$\approx -8.6023 \times 10^{-4}$	≈ -21.1558
2,000	$\approx -8.6023 \times 10^{-5}$	≈ -21.1558
10,000	$\approx -1.7205 \times 10^{-5}$	≈ -21.1558

Table 5: **MSE values**

number of Fourier modes	MSE
200	$\approx 0.192276077317043$
$10,000$	$\approx 0.192276132208228$

table of Fourier coefficients for the truncated smooth polynomial approximation to the flight data up to time stamp $t = 450$

Table 6: **Fourier cosine coefficients**

number of Fourier modes	maximum Fourier mode	minimum Fourier mode
200	≈ 0.3139	$\approx 7.928 \times 10^{-6}$
$2,000$	≈ 0.3139	$\approx 7.857 \times 10^{-8}$

Table 7: **Fourier sine coefficients**

number of Fourier modes	maximum Fourier mode	minimum Fourier mode
200	≈ 21.124	$\approx 2.466 \times 10^{-3}$
$2,000$	≈ 21.236	$\approx 2.466 \times 10^{-4}$

Table 8: **MSE values**

number of Fourier modes	MSE
200	≈ 560.79416
$2,000$	≈ 561.902567337
$10,000$	≈ 5.62001093

Beyond the numerical results portrayed above, the plots below also demonstrate the distribution of higher frequency terms that could be used in the Fourier series expansion, where the computations of the Fourier coefficients are carried out for $10,000$ Fourier sine and cosine coefficients. Due to the significantly higher MSE associated with the Fourier sine coefficients for this example flight, we will only employ the Fourier cosine coefficients in the expansion. Furthermore, to analyze properties of such an expansion from which the MSE will be computed for all corresponding Fourier coefficients used in the expansion, the behavior of the series expansion will be plotted for each of the 4938 **total** time stamps in the flight, where the first time stamp is assigned to the time $t_i = 401.3$, while the last time stamp is assigned to the time $t_f = 473.31$.

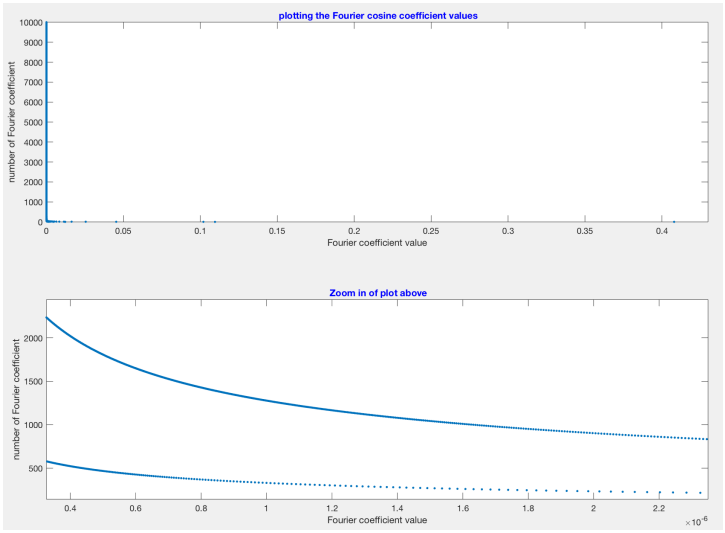

(ABOVE) *Figure 9*: The plots above demonstrate the distribution of computed values of each of the Fourier coefficients. That is, in the first plot in the diagram, a broad inspection of all of the values of the Fourier coefficients demonstrates that there is a threshold frequency, for the naturals n used to compute each Fourier sine and cosine coefficient, beyond which the corresponding Fourier coefficient arbitrarily approaches 0. In the second plot, a zoom in of the first plot demonstrates the threshold beyond which the Fourier coefficient computed past the demarcated numerical frequency in the plot approaches 0.

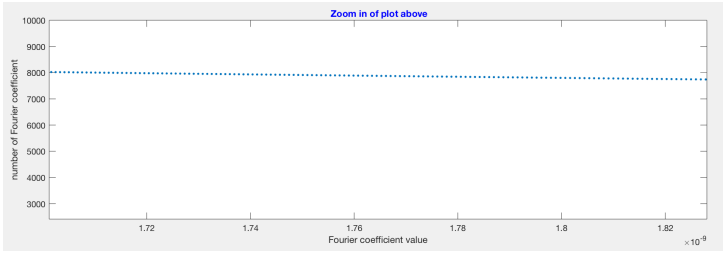

(ABOVE) *Figure 10*: Upon closer examination, what appears to be completely solid blue curves in the previous plot reflects the close proximity of Fourier coefficients of neighboring frequencies.

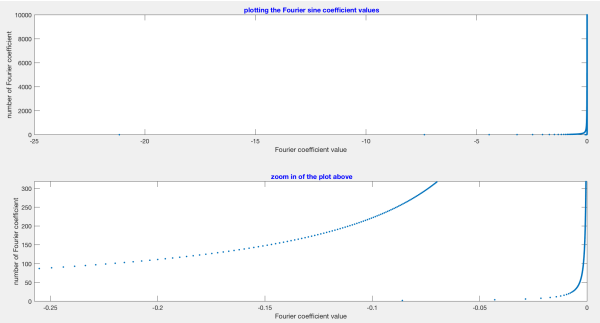

(ABOVE) *Figure 11*: To illustrate similar relationships between the behavior of the Fourier cosine coefficients, the plot above demonstrates the behavior for the sine coefficients of the Fourier series, for as the frequency of the oscillations of the sine term increase. In the first plot, each of the $10,000$ Fourier sine modes are exhibited, which are negative and approach 0 for higher frequencies. In the second plot, a zoom in of the coefficients provided in the previous plot demonstrates that the sine Fourier coefficients for the quadratic approximation taken up to the $t_f \approx 473.3$ time stamp. In comparison to the plot of the Fourier sine coefficients that will be provided for the truncated polynomial approximation of the flight data up to the 450 time stamp.

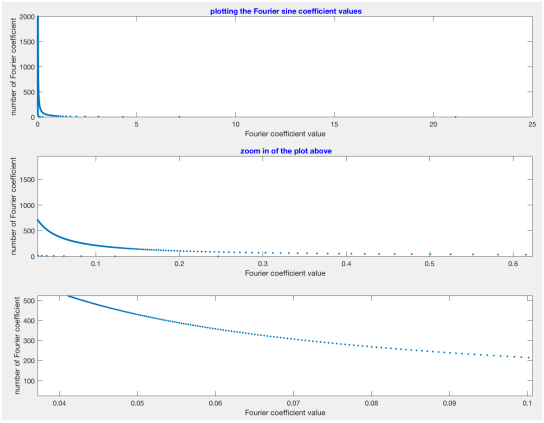

(ABOVE) *Figure 12*: In contrast to the previous diagram for the Fourier sine coefficients, the Fourier sine coefficients, for the truncated polynomial approximation up to the time stamp 450 before the current change occurs results in coefficients that are of opposite sine than those previously presented in the previous diagram. Although the coefficients in the first plot are qualitatively similar to those given in the previous diagram, they are of the opposite sign which nevertheless result in the same MSE. On the other hand, in the second and third plots, we observe the same quantitative behavior in the magnitude of the Fourier coefficients computed for a given frequency. Particularly, the Fourier coefficients that will be used in plots of the series representation that will follow demonstrate that past a fixed frequency n, the Fourier coefficients for all frequencies past the threshold rapidly approach 0.

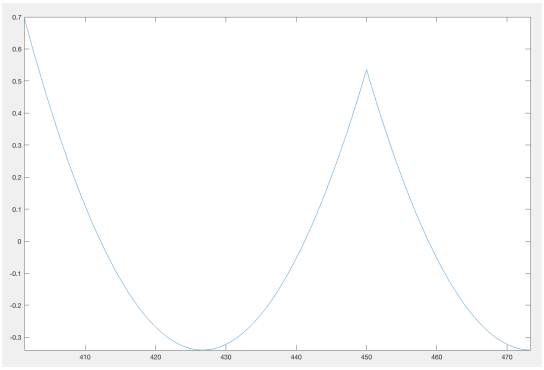

(ABOVE) *Figure 13*: To more closely analyze the behavior of the series approximation from which predictions will be generated with a specified, attributable MSE, the behavior of the series approximation, as t varies linearly with respect to the time stamp which is incremented by a unit for each successive time stamp along the array, is depicted above. As one can anticipate, the behavior of the series approximation can be studied to generate flight predictions by making use of the Fourier series representation as a smooth approximation of the experimental flight data. With such a periodic extension, we are able to achieve specific MSE values by computing the sum of squares of the Fourier coefficients, over the number of coefficients that are implemented in the expansion.

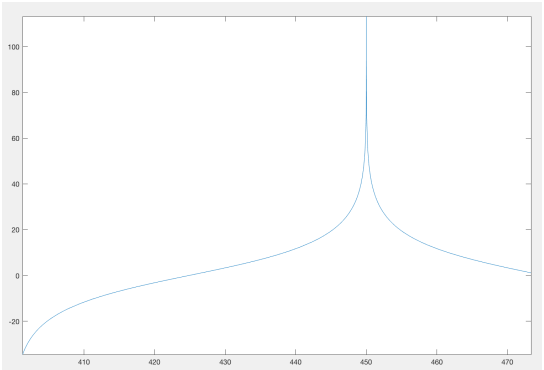

(ABOVE) *Figure 14*: Sine approximation corresponding to the smooth polynomial approximation for the flight data. As indicated from the MSE table values, we do not expect that incorporating such an approximation of the flight data by making use of the sine Fourier coefficients will be useful, because the MSE for these set of coefficient, in comparison to the MSE for the Fourier cosine coefficients, is extraordinarily higher. Additionally, in contrast to the plots of the Fourier sine coefficients that were generated with $10,000$ modes, we observe that taking the time stamps of the flight in this stage only up to 450 still does not benefit our ability to generate predictions.

4.5. a note on adjusting the free parameters in the exponentially decaying factor

From the description and implementation of the auxiliary algorithm as a proxy for the change in $C_{\max}$ across a single flight, from the given fixed ordering of the time stamps and the current measurements as the flight progresses, the assignment

$$\Phi : \mathbf{R}^+ \longrightarrow \mathbf{R}^+ : |t_j - t_k| \mapsto \beta_i \, ,$$

for $j \neq k$, and $\beta_i > 0$, obtains a monotonic pairing of the time intervals of each stage of the flight with the freely chosen β_i, so that, throughout the vriable duration of a given flight pattern:

- periods of shorter duration, in which the magnitude of the current $\mathcal{I}$ abruptly changes, are multiplicatively weighed more unfavorably in the discharge of capacitance of the circuit in the engine, while
- periods of longer duration, in which the current of magnitude $\mathcal{I}$ changes more gradually over the course of a stage in the flight, are multiplicatively weighed more favorably in terms of the impact on the maximum capacitance that the circuit can hold, and therefore, less adversely impact the circuit.

With such a convention of the free parameter assignment in hand, a range of exponentially decaying factors, and hence, of the maximum discharge of capacitance in the circuit, predictions can be realized. By means of providing examples of flight patterns for which the time intervals of each stage will be collected, from which the temporally adjusted weighted exponential decrease of the battery will be computed, consider the following sequence of flights from publicly available NASA prognostic repository #15.

4.6. example from Set 3 HRF: identifying thermal stress on the engine during the beginning and ending stages of the flight

In addition to specifying the β_i parameters for which $\mathcal{I}$ undergoes a change in magnitude in the intermediate stages of the flight, the beginning and ending stages of each flight are of additional interest in choosing β free parameters to inform the choice of the exponentially decaying $C_{\max}$. In the 2 examples from Set 3 given below, we will repeat the same steps of the auxiliary algorithm that is provided earlier in the report, which include:

- per the convention through Φ, assigning larger β parameters for the stages of the flight during which the duration of that specific stage of the flight is longer, ie has more time stamps,
- exponentially weighing shorter and longer periods of the flight appropriately against one another so that the exponential decay in $C_{\max}$ across sequences of flights
- generate predictions for future flights by combinatorially permuting the stage, in addition to the magnitude of the parasitic load, to be defined in future sections.

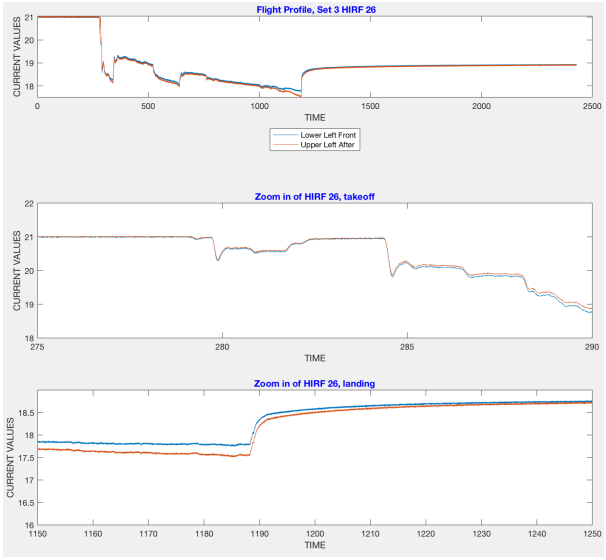

(ABOVE) *Figure 15*: In the example flight from Set 3 HRF, the individual current measurements from the lower left and upper right arms of the circuit are plotted for identical time stamps over which measurements are collected. In the calculations of the exponential change in $C_{\max}$ that will follow, the beginning and ending time

periods of each flight will also be factored into the power of the exponential, given the initial capacitance, so that the strain from the beginning and ending stages of the flight can also be accounted for, which also account for the decay in $C_{\max}$.

5. PROCEDURE FOR GENERATING THE COMBINATORIAL SPACE OF FLIGHT PREDICTIONS

5.1. general remarks

To produce effective, and informative, flight predictions given a numerically specified exponential rate of decay in $C_{\max}$, we will proceed with the following steps:

- Step 1 (**identifying the stage of the flight during which the prediction is to be established**): To systematically address all stages and times during which an anomaly could occur, whether through the flight plan or through a parasitic load of the circuit which grows exponential or polynomially with respect to time which will be distinguished in future steps, we will introduce arbitrary time stamps $t^{(i)}_{\text{abort}}$ corresponding to each stamp $T^{(i)}$ of a given flight. From such time stamps in future flight plans that we designate as attributable to anomalies in the flight plan, predictions for the flight in question will be generated by:
  - linearly varying the stamp $t^{(i)}_{\text{abort}}$ forwards in time for all admissible times in the stage $\mathcal{T}^{(i)}$ of the flight,
  - combinatorially incorporating the minimum and maximum rates of exponential decay in $C_{\max}$ of the circuit, by means of introducing a suitable range of free parameters β_i in the exponentially decaying factor, insofar as to not only simulate varying rates of exponential decrease in the ability of the circuit to transport current, but to also account for flight plan anomalies in **each** stage of the flight,
  - enforcing predictions for whether the flight should be terminated, by determining at which time stamp $t^{(i)}_{\text{SOC}} < t^{(i)}_{\text{abort}}$ the flight should be terminated, in order for the flight to maintain the 30% state of charge threshold discussed in Hogge et al 2015.
- Step 2 (**computing informative ranges of the exponential decay of** $C_{\max}$): In order to pursue realistic predictions, we must also introduce upper and lower bounds for the exponential decay in $C_{\max}$. Pursuant of this goal, we wish to measure the change in exponential decay that we can attribute to a different choice of parameter β_j, say β'_j, satisfying $|\beta_j - \beta'_j| < \epsilon$ for arbitrary $\epsilon > 0$. From such a choice of a different parameter β'_j, the exponential factor for measuring the change in capacitance $C_{\max}$, across consecutive cycles, is of the form,

$$e^{\overbrace{\sum_{i\cap j}\beta_i\left(t^{(i)}_{\text{final}}-t^{(i)}_{\text{initial}}\right)+\beta_j\left(t^{(j)}_{\text{final}}-t^{(j)}_{\text{initial}}\right)}^{\text{for first choice of }\beta_j}-\overbrace{\sum_{i\cap j}\beta_i\left(t^{(i)}_{\text{final}}-t^{(i)}_{\text{initial}}\right)+\beta'_j\left(t^{(j)}_{\text{final}}-t^{(j)}_{\text{initial}}\right)}^{\text{for second choice of }\beta_j}},$$

where the real parameters β_j, β'_j are chosen during the stage $T^{(j)}$ of the flight, which has time duration $t^{(j)}_{\text{final}} - t^{(j)}_{\text{initial}}$. Because all of the remaining β_i, for $i \neq j$, are left fixed, enforcing a different choice of the β_j parameter amounts to a multiplicative, exponentially decaying factor, of the form,

$$e^{\sum_{i\cap j}\beta_i\left(t^{(i)}_{\text{final}}-t^{(i)}_{\text{initial}}\right)}\left(e^{\left(\beta_j-\beta'_j\right)\left(t^{(i)}_{\text{final}}-t^{(i)}_{\text{initial}}\right)}\right),$$

which illustrates how the exponential decay of $C_{\max}$ is dependent on the weight of each β_i, which is tuned for each $\mathcal{T}^{(i)}$. Additionally, to make even more explicit the dependence of time, we will designate the arbitrary time stamps $t^{(i)}_{\text{abort}}$ as the times during each stage $\mathcal{T}^{(i)}$ during which the flight could be terminated, and more precisely, the time stamp in this stage of the flight during which the flight will exactly satisfy the SOC threshold that will be discussed at further length.

- Step 3 (**choosing flight data from the prognostics repository to compute exponential rates of decay in** $C_{\max}$**, from which bounds on the** $C_{\max}$ **will be obtained**: With remarks concerning how one would expect the $C_{\max}$ of the circuit to change across successive flights from the choice of each β_i, as a consequence it is important to designate the sets of experimental data from which exponential rates of decay in $C_{\max}$ will be computed. As a rough analogy to training phases in machine learning methods for prognostics which input particular values to an algorithm to obtain a desired output, a similar initial phase of the algorithm will be implemented, so that feasible lower and upper bounds for the $C_{\max}$ will generate predictions given arbitrary time stamps $t^{(j)}_{\text{abort}} \in \mathcal{T}^{(j)}$ for the stage $\mathcal{T}^{(j)}$, again given com-

pletely arbitrary time stamps at which the flight can be aborted, either due to flight plan anomalies or mechanical failures in the circuit of the engine which will be distinguished in upcoming comments. Towards fulfilling this goal, we have included plots below that are indicative of the rates of decrease in $C_{\max}$ across sequences of flights that are given by Sets 3, 4, 5 and 6 from the online NASA data prognostics repository. Particularly, in the plots that will follow, we will carry out similar steps in computing and numerically representing the decay in $C_{\max}$ due to varying expressions due to the polynomial and exponentially varying parasitic loads that are dependent on time.

- Step 4 (**beyond choosing the flight data: generalizing sets of predictions in flight plan abnormalities given a time stamp of flight termination**): With upper and lower bounds for $C_{\max}$ in hand, generating flight predictions now amounts to:
  - Implementing the user-defined time during which an arbitrary flight plan is to be aborted, due to either flight plan abnormalities or mechanical failures associated with the circuit, namely by choosing each possible stage of the future flight plans at which the anomaly could occur, and even more so, by accompanying rates of decay in the maximum capacitance,
  - generalizing the notion of abortions of a flight due to unforseen changes in the $C_{\max}$ value of the circuit, with the addition of another exponentially decaying factor appended to the exponential factor has has already been given and discussed, which is of the form,

$$\mathcal{C}^{\mathrm{PL},\mathcal{T}^{(i)}}_{\max_{i+1}} = \left(e^{\sum_i -\beta_i |t^{(i)}_{\text{initial}} - t^{(i)}_{\text{final}}|} \times e^{\beta^{\mathrm{PL},\mathcal{T}^{(i)}}_{\mathcal{T}^{(i)}_{\mathrm{PL}}} |{t^{PL}}_{\text{final}} - {t^{PL}}_{\text{initial}}|} \right) C_{\max_i} ,$$

which denotes the local exponential decay of $C_{\max}$ given a temporally dependent, exponentially increasing, parasitic load PL. Numerically, it is important to remark upon the nature of this exponential appendant, in the sense that the power of the exponential that is added onto the exponential can either be equal, less than, or greater in magnitude than the summation in the power of the first exponential that is dependent on both the β_i and duration of each stage $\mathcal{T}^{(i)}$ of the flight. In the second exponential decaying factor in the expression for the local capacitance $\mathcal{C}$ above, the free β parameter with the subscripts $\mathcal{T}^{(i)}$ and $\mathcal{T}^{(i)}_{\mathrm{PL}}$ are indicative of the free parameter choice that the user can himself or herself tune to the rate at which the parasitic load is negatively impacting the ability of the circuit to transport current optimally. At with the previous construction of the exponentially decaying factor for $C_{\max}$ that has been highlighted, the β^{PL} free parameter is multiplicatively associated with the time interval at which PL is injected. On the other hand, one may similarly define the decay of the local capacitance due to a polynomial factor, instead of an exponential one, which is of the form,

$$\mathcal{C}^{\mathrm{PL},\mathcal{T}^{(i)}}_{\max_{i+1}} = \left(e^{\sum_i -\beta_i |t^{(i)}_{\text{initial}} - t^{(i)}_{\text{final}}|} \times \left(1 + (\beta^{\mathrm{PL},\mathcal{T}^{(i)}}_{\mathcal{T}^{(i)}_{\mathrm{PL}}} |{t^{PL}}_{\text{final}} - {t^{PL}}_{\text{initial}}|){t^{PL}}_{\text{final}} + (\beta^{\mathrm{PL},\mathcal{T}^{(i)}}_{\mathcal{T}^{(i)}_{\mathrm{PL}}} |{t^{PL}}_{\text{final}} - {t^{PL}}_{\text{initial}}|) \frac{({t^{PL}}_{\text{final}})^2}{2} + \cdots \right) \right) C_{\max_i} ,$$

for a parasitic load, polynomially increasing, which impairs the $C_{\max}$ value of the circuit, injected upon the circuit in stage $\mathcal{T}^{(i)}$ of the flight with corresponding choice of free parameter α_i for $i \in \mathbf{N}$. Numerically, we observe that as with the expression of the local capacitance decay with the appended exponentially decaying factor for PL, the polynomially decaying factor that is appended to the exponential factor for $C_{\max}$, in the second expression, can be adjusted so that the rate at which the polynomially increases with respect to time is either greater than, less than, or equal to the decay with respect to time of the exponential factor. Nevertheless, the choice of the free α_i parameter, when added to the exponentially decaying factor for computations of the rate of decay of the **usual** capacitance $C_{\max}$, allow for different combinations of the rate of decay in the capacitance, given a particular stage of the flight. In what follows, we will also present how to carry out computations relating to the accompanying SOC of the battery, from expressions of $\mathcal{C}$ given above.

- Step 5 (**SOC formulas based on formalisms of the maximum capacitance for the regular and local cases**): From expressions of $C_{\max}$ and $\mathcal{C}^{PL}$, we can make use of the formula for computing the SOC to propose 3 different formulas that can be used to compute the corre-

sponding state of charge, each of which are of the form,

$$\mathrm{SOC}_1 = 1 - \frac{q_{\max} - q_b}{e^{\sum_i -\beta_i \times t^{(i)}_{\text{initial}} - t^{(i)}_{\text{final}}} C_{\max}},$$

$$\mathrm{SOC}_2 = 1 - (q_{\max} - q_b)/[e^{\sum_i -\beta_i |t^{(i)}_{\text{initial}} - t^{(i)}_{\text{final}}|} \times e^{\beta^{\mathrm{PL},\mathcal{T}^{(i)}}_{\mathcal{T}^{(i)}_{\mathrm{PL}}} |t^{PL}{}_{\text{final}} - t^{PL}{}_{\text{initial}}|} C_{\max}]$$

$$\mathrm{SOC}_3 = 1 - (q_{\max} - q_b)/[1 + (\beta^{\mathrm{PL},\mathcal{T}^{(i)}}_{\mathcal{T}^{(i)}_{\mathrm{PL}}} |t^{PL}{}_{\text{final}} - t^{PL}{}_{\text{initial}}) t^{PL}{}_{\text{final}} + (\beta^{\mathrm{PL},\mathcal{T}^{(i)}}_{\mathcal{T}^{(i)}_{\mathrm{PL}}} |t^{PL}{}_{\text{final}} - t^{PL}{}_{\text{initial}}) \frac{(t^{PL}{}_{\text{final}})^2}{2} + \cdots) C_{\max}],$$

respectively, each of which correspond to the SOC for the first formula for the capacitance introduced the earliest in the report, while the remaining 2 formulas below the first SOC equation denote expressions for the SOC due to the local capacitance $\mathcal{C}$ of the parasitic load, with either exponential rate of decay, or exponential-polynomial rate of decay.

- Step 6 (**summarizing the procedure: backtracking from t_{abort} to determine the intervals of time for which the current satisfies 30% SOC**): From either a flight or parasitically driven mechanical abnormality, we can make flight predictions by following the previously mentioned steps, in which exponentially weighing the duration of each flight, as mechanical or thermal stress on the engine, provides convenient interpretations for the total duration of a flight before falling before the SOC **threshold**.

5.2. further remarks on the rate of decay of the local capacitance due to a parasitic load

To generate meaningful computations of flight predictions that are dependent on the capacitance, in addition to the specific decay at which the capacitance is decaying given a specific flight trajectory, we inject a varying polynomial and exponential term additively to the maximum capacitance, which contributes to the accelerated rate of decay in the circuit engine. In particular, this general framework allows for both great flexibility not only in the position at which a mechanical malfunction in a given flight occurs, but also in the numerical magnitude with which the maximum capacitance decays over the remaining course of a flight, or future flights. To illustrate the power of this approach in generating much broader combinatorial spaces of flight predictions in comparison to statistical modeling approaches, either through neural networks, random Forest, or Lowess fit, each of which rely on variations of linear regression or machine learning esche techniques to train the models to output a desired flight prediction that is deemed reasonable, we will highlight different scenarios in which the parasitic load is injected into the circuit, from which the decay of the maximum capacitance will be calculated. Depending on the rate of polynomial or exponential decay that is specified as a parasitic load for the circuit, flight predictions corresponding to this rate of decay in the maximum capacitance will be calculated according to the 30% SOC threshold as enforced in the 2015 paper. With such an exponential, or polynomial, decay in capacitance, flight predictions for upcoming flights, or segments of flights, will be generated by determining the point at which the capacitance, with the rate of decay which is time dependent on the duration of each stage in the given sequence of flights, will fail to satisfy the 30% threshold.

To realistically ensure that the flight will be able to land at the maximum time stamp at which the 30% threshold is satisfied, the rate of change of the SOC threshold will be calculated backwards in time from the maximum time stamp at which the flight will fail to satisfy the threshold requirement if it were to continue flying. With computational results, reliant on appropriate choices of the /beta parameters in the exponentially decaying temporal factor, we produce similar results surrounding the exponential and polynomial terms which are added onto the maximum capacitance across the sequence of flights from publicly available HRF data sets in the NASA repository. With varying rates of decay, one can easily generate reliable flight predictions for typical parasitic loads that are placed into a flight, by specifying the point in time at which the parasitic load is to be injected as an exponential, or polynomial, burden on the ability of the circuit to perform mechanical work, and hence fly normally, in addition to the ability of the circuit to continue satisfying the SOC threshold. From the downward sloping rays, each of which is reflective of different rates of decay in the capacitance due to the parasitic load, such exponential and polynomial rates of decay directly reflect the maximum duration of flight times for the flight following the moment at which the load is imposed onto the circuit.

From typical speeds at which the motor operates and is able to change directions of motion from experimentally collected current readings throughout each flight in a given sequence, which can be straightforwardly computed by finite differencing across the distances over which the aircraft is displaced through mechanical work

performed by the engine divided by corresponding intervals of time, one can introduce distance inequalities depending on the rate of decay in the maximum capacitance for future flight plans. At this step of the implementation, it is important to emphasize that, as evidenced through the rate of decay of the maximum capacitance, that the maximum distance at which the aircraft can continue to fly beyond the the moment at which the parasitic load is injected is inversely proportional to the magnitude of the load itself. Furthermore, if one wants to generate flight predictions for a sequence of flights which are either temporally identical to all stages of the flights in the sequence which are used to compute the rate of decay in the maximum capacitance that is initially provided before the parasitic load is injected, then one would immediately expect that the aircraft would not be able to undergo the same sequence of flights because the maximum capacitance of each flight across the same sequence would decay more quickly given any nonzero, temporally dependent factor that is added to the rate of decay of the maximum capacitance.

As suggested through computations in the table above, we are able to readily generate predictions for upcoming flights by specifying the stage of the flight at which the load is imposed, from which computations of the local capacitance, due to either polynomial or exponential decay, will be calculated. Thus, from such a rate of decay, it is possible to establish suggestions for the maximum flight time given the duration of each stage of the flight. Conversely, past flight data from previous mechanical malfunctions could also be interpreted, with the following approach. If the duration for either a mechanical malfunction or flight anomaly is known in a flight, an implementation the magnitude of the parasitic load, whether polynomial or exponential, can be computed by working backwards from the expressions given in the previous section. Namely, if the distance over which the mechanical or flight plan anomaly is known through experimentally gathered current measurements, then the distance over which the anomaly has occurred can be used to approximate the magnitude of the parasitic load responsible for the anomaly. Furthermore, because an exponentially varying parasitic load that increases with time can be Taylor expanded into a polynomial of fixed degree, backwards calculations from the distance over which a flight anomaly have occurred could also be implemented to obtain a polynomial expression for the parasitic load that is responsible for the anomaly, whatever its type may be. In either circumstance, the approach fits within experimental data that is to be gathered, or has been gathered, to inform maintenance for future flights. Clearly, if the magnitude due to the parasitic load is sufficiently dominant, in the sense that the degradation due to the load prevents the flight from completing individual stages of a flight that are of the same duration from flights that it has already completed previously in a given sequence, then the flight should immediately land, and moreover, from the collections of current measurements throughout previous flights, be examined in the lab to determine the origin and extent of damage of the parasitic load on the entire circuit.

6. CONCLUDING REMARKS

To conclude, the methods and discussion that have been brought forth in this paper demonstrate the following. By introducing an exponentially decaying factor that is temporally weighed in specific sets of current versus time measurements that are experimentally recorded for different flights, we are able to generate widely accommodating flight predictions that take into account the specific nature of the data, in this case the current that is supplied to the engine throughout a flight, which is variable and can most certainly degrade with repeated use. In future work, we are continuing to pursue our interest of being able to continue generating sufficiently large combinatorial spaces from the Φ assignment. Furthermore, although the mapping is defined so that we do not assign multiple β free parameters to the $C_{\max}$ decay for time periods of a flight that are not equal, there are countably many mappings that we can construct to further experiment with the steepness of the $C_{\max}$ decay which could be of additional interest for aircrafts that are either built according to different specifications than the one in which chamber experiments were held. Certainly, the methodology and the approach presented here is able to address such changes in machinery by being able to explore families of Φ mappings, namely a function space of mappings $\Phi_{\mathcal{S}}$, where $\mathcal{S}$ is the sample space of times during individual stages of the flight. With a more general notion of the rate of change of the maximum capacitance with respect to not only the flight number of a cycle but also to the hardware specific requirements of the battery and equipment that are being used.

Another area of interest for future work includes being able to develop more specifications for other data structures that could arise in the experimentally gathered current readings in types of truncated plots that are returned by the auxiliary algorithm as given in the appendix. With more complicated experiments and specifications either to the amount of current that will be delivered during a flight, or even on the duration of the flight itself, it would be helpful to continue expanding on the approach to make it more versatile to handle flights with an arbitrary number of stages, which could improve battery maintenance, as well as overall construction of the aircraft, for optimal aerodynamic performance in a wide variety of flight patterns. Although the estimates for the

decay in the maximum capacitance will not be subject to electromagnetic radiation effects that are present in the background of the environment which can have a significant impact on the temperature at which the equipment operates, another exponential factor with its own free parameter accounting for the difference between the ambient temperature of the environment, and the maximum temperature at which the battery will continue to carry sufficient enough current above the SOC threshold, can be implemented.

7. APPENDIX: DEMONSTRATION OF HOW TO GENERATE THE COMBINATORIAL SPACE FROM GIVEN TRENDS IN THE DECAY OF THE CAPACITANCE

7.1. outline of the steps

1.) To carry out the methods discussed at length so far, the following steps will be carried out:

- plot each flight, obtain the truncated flight plan from the auxiliary algorithm,
- from the approximate times returned by the auxiliary algorithm obtain the appropriate time intervals for the $C_{\max}$ decay,
- obtain polynomial approximation of flight data, with roots r_i and stretching constant k,
- compute the Fourier coefficients, series representation and MSE from the Fourier coefficients,
- generate different sets of flight predictions depending on the magnitude at which the parasitic load is injected into the flight, from which adjustments to the exponential decay of the $C_{\max}$ will be determined.

2.) As a recapitulation of previous remarks, in the plots and steps that will be executed below, we will generate flight predictions by:

- incorporating values that the current levels off at near the end of each flight,
- concatenating time and current vectors into a combined vector so that associations between current readings and the time at which such readings are collected can be easily established,
- isolating the stages of each flight between collections of time stamps over which the current is either constant or is monotonically decreasing,
- from the demarcated stages of each flight, proceed to compute the roots and stretching constant of the smooth polynomial approximation for each stage of the flight,
- generating flight predictions, for plans of varying composition, either of Type 1 or Type 2.

3.) After establishing the polynomial approximations through the interpolating root finding method:

- from endpoints of the polynomial approximation defined over the endpoints corresponding to the beginning and ending stages of each stage of the flight, straightforward characteristics of the root finding scheme allow for
  - reportable MSE values which are computations of statistical significance that can be carried out by computing the sum of the squares of the Fourier coefficients from the smooth polynomial approximation of the flight stage in question,
  - comparison of different MSEs across unique stages of individual flights as a reflection of the accuracy of predictions for future flights

7.2. prognostics commentary

In the charts and tables that follow, we enact the steps of the auxiliary algorithm so that we may construct exponentially decaying factors which predict how the maximum capacitance will vary within neighboring flights of a given cycle. Because we chose the polynomially decaying parasitic load as a multiplicative factor for $C_{\max}$ which is composed of lower order terms in the series expansion of the exponentially decaying quantity for the other form the parasitic load, upper and lower bounds for the $C_{\max}$ decay for the exponentially decaying parasitic load produce informative ranges, approximately the same as those generated by the linear expansion of the exponential. To ensure that the results that are populated within each table are reproducible from the publicly available data, the plot of the truncated flight plan returned by the auxiliary algorithm is reproduced. Then, from the truncated flight plan, approximate intervals of the duration of each stage of the flight are given. Although values for the SOC are not explicitly provided in the remaining pages of the report, the upper and lower bounds for $C_{\max}$ nevertheless provide a range of the time stamp values for each stage of a given flight, in addition to the range of free β which can be used to vary the SOC within the flight. Numerically, if one were to enforce on set of free β in the exponentially decaying capacitance formulae provided for the exponentially and polynomially decaying parasitic loads, it is possible that the SOC could decay too quickly and would not capture the performance of the battery to sustain charge over multiple cycles. To avoid implementing free parameter choices into the model that are not instructive for generating predictions, legitimate parameter choices for the model in-

clude β, approximately of the magnitude that is given in the table below for example flights, of order between $\frac{1}{1800}$, corresponding to shorter stages of a flight, to $\frac{1}{150}$, corresponding to longer stages of a flight, so that the $C_{\max}$ of the battery will decay moderately enough, insofar as to mimic the real time decay of the battery that has been confirmed through laboratory experiment.

7.3. enacting the steps for Set 3 HRF

HRF 22

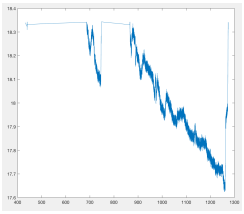

The tables below demonstrate the range of β parameters that would be reasonable to model a range of decay for the maximum capacitance of the battery. With these numerical values, we can observe a range of decay of $C_{\max}$ whose range is around 5%, in addition to the PL classification in the following table which demonstrates the initial times at which the parasitic load is injected, in addition to the β value that we implemented into the exponentially decaying factor for the parasitic load. With the values that we have given in the tables and for other flights for the first 3 sets, we are able to obtain additional rates of decay in $C_{\max}$ depending on the magnitude of the β parameter, in addition to the stage of the flight at which the PL is injected. Intuitively, the β free parameter and t_{init} allow for us to weigh, and relatively compare, the different rates of possible exponential decay for the parasitic load is it either poses a threat to the battery's ability to impact the circuit's capacitance in a flight. With parameter choices which do not result in exponential decay that is too steep, introducing additional sets of β parameters in the exponentially decaying factor, with the $\%$ capacitance left over from the circuit from the previous flight as the starting point for $C_{\max}$ in the neighboring flight in a flight sequence.

stage number	duration of stage, in seconds
1	≈ 200
2	≈ 400

Φ β value stages 1,2	$\%$ $C_{\max}$
$\frac{1}{2000}, \frac{1}{1500}$	≈ 0.693
$\frac{1}{1800}, \frac{1}{1200}$	≈ 0.641

flight plan type	PL classification	t_{init}, β
A	exp	$\approx 670, \frac{1}{10000}$
B	exp	$\approx 880, \frac{1}{8000}$

bounds on $C_{\max}$ decay
$0.87712 \leq C_{\max} \leq 0.88692$
$0.60991 \leq C_{\max} \leq 0.65924$

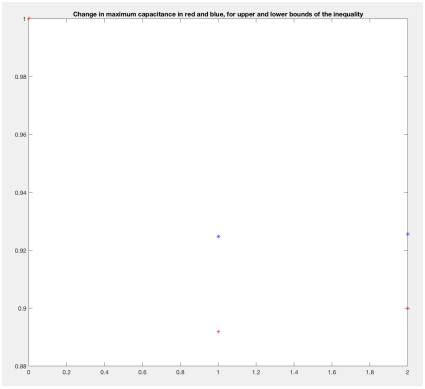

From the SOC plot, it is possible to generate predictions for the flight which are related to the ability of the circuit to not degrade quickly, which is directly correlated to the ability of the circuit to carry charge which is time dependent for the maximum durations of flight trials that can be conducted. From example numerical results illustrated in the bound of $C_{\max}$ above, we substitute the capacitance into the denominator the the 3 SOC expressions given in a previous section. From the particular values of the intrinsic $C_{\max}$ values that are specific to each possible battery that could be used in the trial, we know that the SOC would decay differently, completely dependent on the maximum capacitance value. Specifically, the red and blue asterisks in the plot above denote that the different possibilities for the $C_{\max}$ value which can be obtained from the upper and lower bounds of the inequality in the third table above. With the numerical settings on the parameters that we have enforced, we can feasibly achieve high precision for the SOC degradation across multiple flights, which is evidenced by the proximity of the SOC current readings, from the change in $C_{\max}$ values, that have been computed with the given parameter choices. From the initial starting point of a $C_{\max} = 0.015$, $q_{\max} = 10^{-3}$ and $q_b = 10^{-5}$, we can compute the corresponding SOC values. The numerical estimates for the SOC values that we have included enable us to generate predictions for the flight, which are of the following nature. If we insert a parasitic load that is exponentially increasing with respect to time at the onset of either the first or second stages of the flight, the

model for computing the exponential decay in $C_{\max}$ can not only reliably generate rates of decay without having to perform laboratory measurements of the battery cell, but can also generate additional trajectories for the flight, and future flights, by penalizing the stage of the flight during which the load is injected. Moreover, with the choice of free parameters that we have introduced for this flight and for the flights that follow below, we are able to generate an exhaustive combinatorial space of all possible outcomes for the flight. If, for an unforseen reason due to a potential mechanical failure, the flight is forced to abort at any fixed time during the flight, the model is able to accommodate for such a preliminary termination, through estimates of the SOC, and overall health of the battery, which can be used to determine the optimal trajectory that an aircraft can use to return to its initial point of origin. Within this mathematical framework, predictions for prognostics purposes may be generated for other flights by determining the rate at which the exponential decay of the maximum capacitance in the battery occurs, from which one can set free β parameters to determine the maximum and minimum rates of decay of the SOC in the battery. From such preliminary estimates, the inequalities can be updated for future flights to reflect the burden, due to thermal stress and other factors, on the battery as long as it continues to satisfy the SOC threshold.

HRF 23

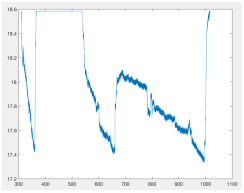

stage number	duration of stage, in seconds
1	≈ 80
2	≈ 180
3	≈ 300

Φ β value stages 1,2,3	% $C_{\max}$
$\frac{1}{950}, \frac{1}{700}, \frac{1}{600}$	≈ 0.4311
$\frac{1}{1500}, \frac{1}{1000}, \frac{1}{800}$	≈ 0.54426

flight plan type	PL classification	t_{init}, β
A	exp	$\approx 310, \frac{1}{5000}$
B	exp	$\approx 550, \frac{1}{3500}$
C	exp	$\approx 680, \frac{1}{8000}$

bounds on $C_{\max}$ decay
$0.9119 \leq C_{\max} \leq 0.94051$
$0.65579 \leq C_{\max} \leq 0.68685$
$0.33195 \leq C_{\max} \leq 0.419051$

HRF 24

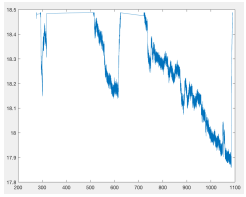

stage number	duration of stage, in seconds
1	≈ 50
2	≈ 140
3	≈ 330

Φ β value stages 1,2	% $C_{\max}$
$\frac{1}{1500}, \frac{1}{1300}, \frac{1}{500}$	≈ 0.44887
$\frac{1}{1300}, \frac{1}{1100}, \frac{1}{450}$	≈ 0.40695

flight plan type	PL classification	t_{init}, β
A	exp	$\approx 280, \frac{1}{5000}$
B	exp	$\approx 480, \frac{1}{8000}$
C	exp	$\approx 730, \frac{1}{3500}$

bounds on $C_{\max}$ decay
$0.95269 \leq C_{\max} \leq 0.95759$
$0.82429 \leq C_{\max} \leq 0.844491$
$0.360287 \leq C_{\max} \leq 0.39740$

HRF 25

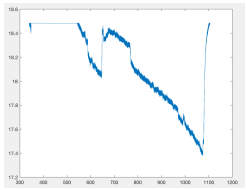

stage number	duration of stage, in seconds
1	≈ 130
2	≈ 520

Φ β value stages 1,2	% $C_{\max}$
$\frac{1}{1400}, \frac{1}{80}$	≈ 0.11385
$\frac{1}{800}, \frac{1}{250}$	≈ 0.10619

flight plan type	PL classification	t_{init}, β
A	exp	$\approx 520, \frac{1}{10000}$
B	exp	$\approx 680, \frac{1}{5000}$

bounds on $C_{\max}$ decay
$0.877058 \leq C_{\max} \leq 0.899553$
$0.001218 \leq C_{\max} \leq 0.094467$

HRF 26

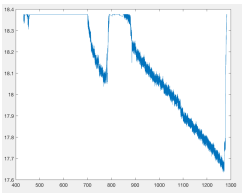

stage number	duration of stage, in seconds
1	≈ 120
2	≈ 370

Φ β value stages 1,2	% $C_{\max}$
$\frac{1}{1000}, \frac{1}{400}$	≈ 0.35169
$\frac{1}{1100}, \frac{1}{300}$	≈ 0.26121

flight plan type	PL classification	t_{init}, β
A	exp	$\approx 680, \frac{1}{10000}$
B	exp	$\approx 870, \frac{1}{8000}$

bounds on $C_{\max}$ decay
$0.87634 \leq C_{\max} \leq 0.88595$
$0.246431 \leq C_{\max} \leq 0.33179$

HRF 27

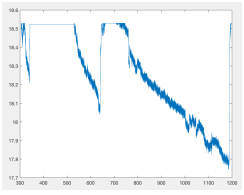

stage number	duration of stage, in seconds
1	≈ 170
2	≈ 150
3	≈ 420

Φ β value stages 1,2	% change in $C_{\max}$
$\frac{1}{1100}, \frac{1}{800}, \frac{1}{350}$	≈ 0.213943
$\frac{1}{1500}, \frac{1}{700}, \frac{1}{250}$	≈ 0.13451

flight plan type	PL classification	t_{init}, β
A	exp	$\approx 280, \frac{1}{5000}$
B	exp	$\approx 480, \frac{1}{8000}$
C	exp	$\approx 730, \frac{1}{3500}$

bounds on $C_{\max}$ decay
$0.8101422 \leq C_{\max} \leq 0.8442227$
$0.659156 \leq C_{\max} \leq 0.668734$
$0.11054 \leq C_{\max} \leq 0.176084$

HRF 28

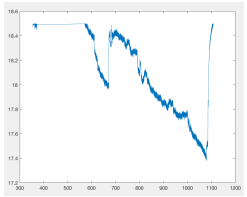

stage number	duration of stage, in seconds
1	≈ 130
2	≈ 430

Φ β value stages 1,2	% change in $C_{\max}$
$\frac{1}{1500}, \frac{1}{540}$	≈ 0.413556
$\frac{1}{1200}, \frac{1}{350}$	≈ 0.262657

flight plan type	PL classification	t_{init}, β
A	exp	$\approx 580, \frac{1}{9000}$
B	exp	$\approx 680, \frac{1}{7500}$

bounds on $C_{\max}$ decay
$0.88446 \leq C_{\max} \leq 0.903832$
$0.2444651 \leq C_{\max} \leq 0.384912$

HRF 29

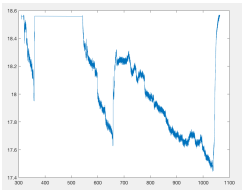

stage number	duration of stage, in seconds
1	≈ 50
2	≈ 170
3	≈ 370

Φ β value stages 1,2	% change in $C_{\max}$
$\frac{1}{2000}, \frac{1}{1700}, \frac{1}{370}$	≈ 0.38781679
$\frac{1}{1500}, \frac{1}{1300}, \frac{1}{350}$	≈ 0.29486271

flight plan type	PL classification	t_{init}, β
A	exp	$\approx 280, \frac{1}{5000}$
B	exp	$\approx 520, \frac{1}{8000}$
C	exp	$\approx 680, \frac{1}{3500}$

bounds on $C_{\max}$ decay
$0.95759214 \leq C_{\max} \leq 0.9656054$
$0.8225446 \leq C_{\max} \leq 0.829427785$
$0.25712069 \leq C_{\max} \leq 0.2830974$

HRF 30

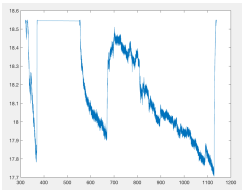

stage number	duration of stage, in seconds
1	≈ 60
2	≈ 130
3	≈ 430

Φ β value stages 1,2	% change in $C_{\max}$
$\frac{1}{1800}, \frac{1}{1500}, \frac{1}{400}$	≈ 0.2986947
$\frac{1}{2000}, \frac{1}{1500}, \frac{1}{450}$	≈ 0.342247123

flight plan type	PL classification	t_{init}, β
A	exp	$\approx 350, \frac{1}{6000}$
B	exp	$\approx 580, \frac{1}{7000}$
C	exp	$\approx 680, \frac{1}{4500}$

bounds on $C_{\max}$ decay
$0.912340924 \leq C_{\max} \leq 0.91545567$
$0.82126885 \leq C_{\max} \leq 0.82401098$
$0.25560372 \leq C_{\max} \leq 0.28707382$

HRF 31

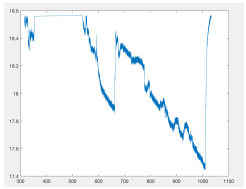

stage number	duration of stage, in seconds
1	≈ 70
2	≈ 140
3	≈ 400

Φ β value stages 1,2	% change in $C_{\max}$
$\frac{1}{2000}, \frac{1}{1700}, \frac{1}{450}$	≈ 0.3655904
$\frac{1}{1800}, \frac{1}{1600}, \frac{1}{400}$	≈ 0.3242019

flight plan type	PL classification	t_{init}, β
A	exp	$\approx 350, \frac{1}{6000}$
B	exp	$\approx 580, \frac{1}{7000}$
C	exp	$\approx 680, \frac{1}{4500}$

bounds on $C_{\max}$ decay
$0.9073543 \leq C_{\max} \leq 0.9108899$
$0.795133 \leq C_{\max} \leq 0.81023502$
$0.267633995 \leq C_{\max} \leq 0.301801$

HRF 32

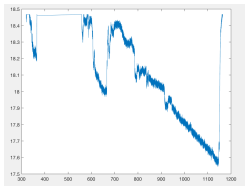

stage number	duration of stage, in seconds
1	≈ 30
2	≈ 140
3	≈ 450

Φ β value stages 1,2	% $C_{\max}$
$\frac{1}{2000}, \frac{1}{1700}, \frac{1}{550}$	≈ 0.4003025
$\frac{1}{1800}, \frac{1}{1500}, \frac{1}{500}$	≈ 0.36421898

flight plan type	PL classification	t_{init}, β
A	exp	$\approx 350, \frac{1}{6000}$
B	exp	$\approx 580, \frac{1}{7000}$
C	exp	$\approx 680, \frac{1}{4500}$

bounds on $C_{\max}$ decay
$0.927743 \leq C_{\max} \leq 0.9292911$
$0.8283385 \leq C_{\max} \leq 0.83888112$
$0.289545 \leq C_{\max} \leq 0.3182306$

HRF 33

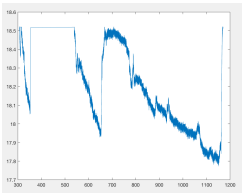

stage number	duration of stage, in seconds
1	≈ 70
2	≈ 150
3	≈ 400

Φ β value stages 1,2	% change in $C_{\max}$
$\frac{1}{1800}, \frac{1}{1300}, \frac{1}{350}$	≈ 0.3572664
$\frac{1}{1500}, \frac{1}{1100}, \frac{1}{200}$	≈ 0.1447090

flight plan type	PL classification	t_{init}, β
A	exp	$\approx 280, \frac{1}{5000}$
B	exp	$\approx 480, \frac{1}{8000}$
C	exp	$\approx 650, \frac{1}{3500}$

bounds on $C_{\max}$ decay
$0.97433509 \leq C_{\max} \leq 0.977588293$
$0.86848932 \leq C_{\max} \leq 0.88899234$
$0.2208010768 \leq C_{\max} \leq 0.300097432$

HRF 34

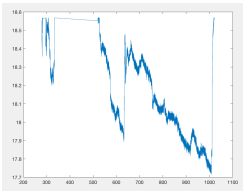

stage number	duration of stage, in seconds
1	≈ 80
2	≈ 200
3	≈ 380

Φ β value stages 1,2	% change in $C_{\max}$
$\frac{1}{1800}, \frac{1}{1500}, \frac{1}{400}$	≈ 0.320683
$\frac{1}{2000}, \frac{1}{1800}, \frac{1}{600}$	≈ 0.4563732

flight plan type	PL classification	t_{init}, β
A	exp	$\approx 270, \frac{1}{5000}$
B	exp	$\approx 530, \frac{1}{8000}$
C	exp	$\approx 670, \frac{1}{3500}$

bounds on $C_{\max}$ decay
$0.9413461 \leq C_{\max} \leq 0.9455391$
$0.7707089 \leq C_{\max} \leq 0.7915377$
$0.2739283 \leq C_{\max} \leq 0.3861399$

HRF 35

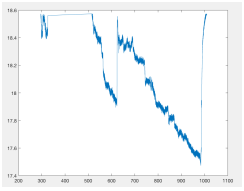

stage number	duration of stage, in seconds
1	≈ 30
2	≈ 120
3	≈ 390

Φ β value stages 1,2	% $C_{\max}$
$\frac{1}{1800}, \frac{1}{1500}, \frac{1}{410}$	≈ 0.3506782
$\frac{1}{1500}, \frac{1}{1200}, \frac{1}{310}$	≈ 0.25206595

flight plan type	PL classification	t_{init}, β
A	exp	$\approx 280, \frac{1}{5000}$
B	exp	$\approx 480, \frac{1}{8000}$
C	exp	$\approx 650, \frac{1}{3500}$

bounds on $C_{\max}$ decay
$0.97433509 \leq C_{\max} \leq 0.977588293$
$0.86848932 \leq C_{\max} \leq 0.88899234$
$0.2208010768 \leq C_{\max} \leq 0.300097432$

HRF 36

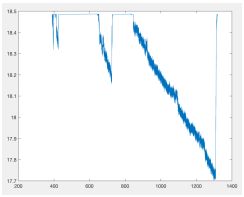

stage number	duration of stage, in seconds
1	≈ 30
2	≈ 70
3	≈ 360

Φ β value stages 1,2	% $C_{\max}$
$\frac{1}{1800}, \frac{1}{1700}, \frac{1}{390}$	≈ 0.3749659
$\frac{1}{1500}, \frac{1}{1200}, \frac{1}{350}$	≈ 0.33058060

flight plan type	PL classification	t_{init}, β
A	exp	$\approx 600, \frac{1}{5000}$
B	exp	$\approx 820, \frac{1}{8000}$
C	exp	$\approx 680, \frac{1}{3500}$

bounds on $C_{\max}$ decay
$0.9743351 \leq C_{\max} \leq 0.97758829$
$0.911111757 \leq C_{\max} \leq 0.92997912$
$0.326600555 \leq C_{\max} \leq 0.333361696$

7.4. enacting the steps for Set 4 HRF

HRF 37

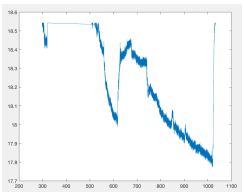

stage number	duration of stage, in seconds
1	≈ 130
2	≈ 400

HRF 38

- excluded because of faulty current-time recordings

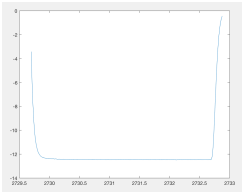

HRF 39

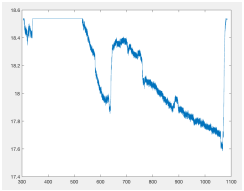

stage number	duration of stage, in seconds
1	≈ 100
2	≈ 430

HRF 40

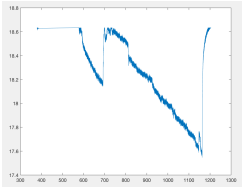

stage number	duration of stage, in seconds
1	≈ 150
2	≈ 430

HRF 41

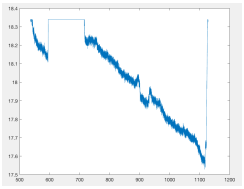

stage number	duration of stage, in seconds
1	≈ 100
2	≈ 430

7.5. enacting the steps for Set 5 HRF

HRF 63

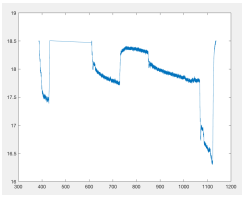

stage number	duration of stage, in seconds
1	≈ 60
2	≈ 100
3	≈ 400

HRF 64

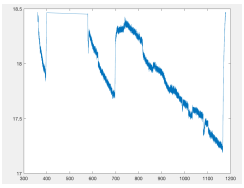

stage number	duration of stage, in seconds
1	≈ 50
2	≈ 180
3	≈ 400

HRF 67

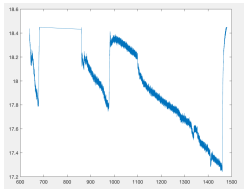

stage number	duration of stage, in seconds
1	≈ 70
2	≈ 150
3	≈ 450

HRF 68

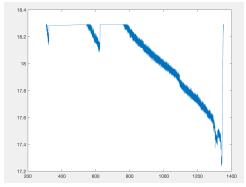

stage number	duration of stage, in seconds
1	≈ 70
2	≈ 550

HRF 69

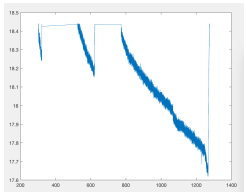

stage number	duration of stage, in seconds
1	≈ 170
2	≈ 350

HRF 71

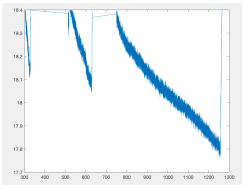

stage number	duration of stage, in seconds
1	≈ 80
2	≈ 160
3	≈ 420

HRF 72

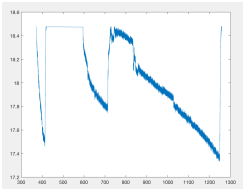

stage number	duration of stage, in seconds
1	≈ 100
2	≈ 150
3	≈ 500

HRF 73

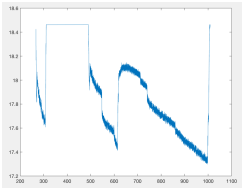

stage number	duration of stage, in seconds
1	≈ 120
2	≈ 140
3	≈ 350

HRF 74

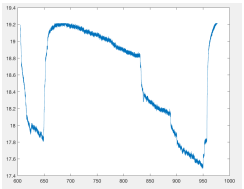

stage number	duration of stage, in seconds
1	≈ 40
2	≈ 170
3	≈ 120

7.6. enacting the steps for Set 6 HRF

HRF 75

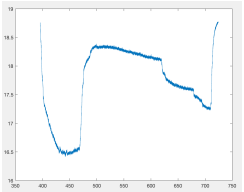

stage number	duration of stage, in seconds
1	≈ 170
2	≈ 300

HRF 76

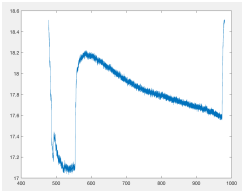

stage number	duration of stage, in seconds
1	≈ 170
2	≈ 400

HRF 77

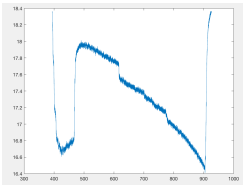

stage number	duration of stage, in seconds
1	≈ 170
2	≈ 400

HRF 78

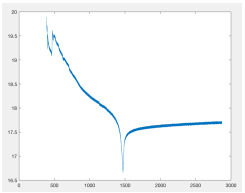

stage number	duration of stage, in seconds
1	≈ 60
2	≈ 700

HRF 81

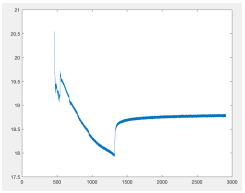

stage number	duration of stage, in seconds
1	≈ 30
2	≈ 700

HRF 79

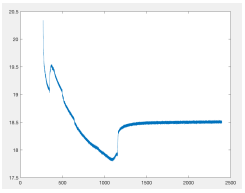

stage number	duration of stage, in seconds
1	≈ 50
2	≈ 800

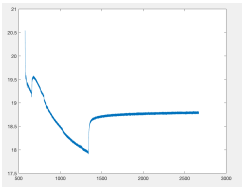

stage number	duration of stage, in seconds
1	≈ 70
2	≈ 650

HRF 80

7.7. brief remarks on the implementation of Cases 1 and 2 from the auxiliary algorithm

From the 2 cases outlined near the beginning of the report to which the auxiliary algorithm have been applied, we remark:

- the auxiliary algorithm for flight plans of Type 1 was executed for Set 3, HRF 22, 23, with a threshold parameter of value 0.5,
- while the threshold parameter was changed to 0.4 for all remaining HRF files up to Set 4, HRF 40,
- to then be changed to 0.35 up to Set 6, HRF 77,
- and finally, the threshold parameter was switches to flights of Type 2, with a threshold parameter value of either 1, or 1.5, for flights HRF $78 - 81$ in Set 6.

From additional tables of $C_{\max}$ values that are provided below each flight plan from which predictions are generated, we also remark that:

- our methods are able to reliably predict future flight times, from a specified duration and number of stages in a given flight, through the exponentially decaying factor for the capacitance,

- predict alternative rates of decay for the maximum capacitance by incorporating different choice of the β factors into the model,
- in addition to being able to account for more complicated flight patterns in upcoming experiments.

7.8. making use of the decay in $C_{\max}$ to generate MSE values and accompanying SOC

From the decay in $C_{\max}$ that we have generated, from each set of β parameters that we have incorporated into the power of the exponential, SOC values can be computed from either the exponential or polynomial parasitic loads that vary with respect to time. To further enhance the ability to generate predictions for different flights, one can make use of the upper and lower bounds from the exponential decay to measure the total predicted time of flights by determining the time at which the SOC fails to satisfy a 30% threshold. From the same threshold that is implemented in [2], as well as many other possible thresholds for flights of varying composition, the methodology is able to capture many different flight plan scenarios, whether a flight plan or mechanical anomaly in the engine emerges to influence the decay in $C_{\max}$, or the duration of the parasitic load in the flight.